

Cross-Camera Distracted Driver Classification through Feature Disentanglement and Contrastive Learning

Simone Bianco, Luigi Celona, Paolo Napoletano

Department of Informatics, Systems and Communication, University of Milano-Bicocca
viale Sarca, 336 Milano, Italy

Abstract—The classification of distracted drivers is pivotal for ensuring safe driving. Previous studies demonstrated the effectiveness of neural networks in automatically predicting driver distraction, fatigue, and potential hazards. However, recent research has uncovered a significant loss of accuracy in these models when applied to samples acquired under conditions that differ from the training data. In this paper, we introduce a robust model designed to withstand changes in camera position within the vehicle. Our Driver Behavior Monitoring Network (DBMNet) relies on a lightweight backbone and integrates a disentanglement module to discard camera view information from features, coupled with contrastive learning to enhance the encoding of various driver actions. Experiments conducted on the daytime and nighttime subsets of the 100-Driver dataset validate the effectiveness of our approach with an increment on average of 9% in Top-1 accuracy in comparison with the state of the art. In addition, cross-dataset and cross-camera experiments conducted on three benchmark datasets, namely AUCDD-V1, EZZ2021 and SFD, demonstrate the superior generalization capability of the proposed method.

Index Terms—Intelligent vehicles, In-vehicle activity monitoring, Driver distraction, Deep learning, Cross camera, Feature disentanglement, Generalization.

I. INTRODUCTION

As of 2019, road traffic accidents are the leading killer of children and youth aged 5 to 29 years and are the 12th leading cause of death when all ages are considered [1]. Traffic accidents pose a growing problem and are projected to rank as the seventh leading cause of global mortality by 2030.¹ According to statistics from the European Road Safety Observatory (ERSO), 5 to 25% of traffic accidents in Europe stem from driver distraction.² The ERSO defines distracted driving as “the diversion of attention away from activities critical for safe driving toward a competing activity, which may result in insufficient or no attention to activities critical for safe driving”. Commonly observed distractions include smartphone usage, eating, or conversing with passengers, all of which heighten the risk of accidents and should be rigorously avoided. Detecting these distracting behaviors through automatic in-vehicle computational systems enables early inter-

vention to avoid distraction-related accidents. In this context, automatic Driver Monitoring Systems (DMS) have emerged as a novel Advanced Driver Assistance System (ADAS) technology to mitigate car accidents [2]. DMSs exploit machine and deep learning techniques and are trained on datasets acquired in both real and simulated scenarios, often with varying protocols and experimental setups [3]–[6]. Significant differences among these setups include the interior configuration of the vehicle, the position and posture of the driver and the camera placement. Consequently, models trained on specific datasets exhibit poor generalization to different data [7]. To deploy these models on non-production embedded systems in various vehicles while maintaining performance, the models must be robust to prior variations. Furthermore, they must generalize to new conditions without increasing computational complexity, considering the limited capacity of the target devices.

This paper addresses the challenge of cross-camera distracted driver classification by introducing the Driver Behavior Monitoring Network (DBMNet). This model is based on the use of a lightweight Convolutional Neural Network (CNN) for encoding RGB images to facilitate its deployment on commercial off-the-shelf devices. To make the model robust across different camera views, we propose a feature disentanglement module. This module separates action-relevant features from view-relevant features, allowing the proposed model to learn high quality features that are invariant to camera and view variations. This is achieved by a weighted combination of the view queries and the feature vector determined by the backbone. The weights are calculated on the basis of the similarity between the test sample and the training views. Moreover, we employ a supervised contrastive learning approach with triplet loss to enhance the learning of disentangled features. While cross-entropy loss theoretically allows the model to discern similarities within categories and differences between them, it does not explicitly guarantee this outcome. In contrast, triplet loss explicitly compels the model to identify similar features for samples within the same category and distinguish features for samples from different categories. In our model, one triplet loss brings representations of different actions captured by the same camera closer together while separating them from identical actions captured by the same camera. This improves the model’s ability to discriminate between different views and enhances the effectiveness of the disentanglement module. Another triplet loss brings representations of identical actions

Corresponding author: Luigi Celona (luigi.celona@unimib.it).

Manuscript received April 19, 2005; revised August 26, 2015.

¹<https://www.who.int/data/gho/data/themes/topics/topic-details/GHO/road-traffic-mortality> (accessed: Jul 31, 2024).

²<https://road-safety.transport.ec.europa.eu/system/files/2021-07/ersosynthesis2018-driverdistracted-summary.pdf> (accessed: Jul 31, 2024).

captured by different cameras closer together while separating different actions captured by the same camera. This aids in the categorization of driver actions.

The proposed work is unique because no previous approach has explicitly addressed modeling invariance in experimental configurations. We adopt a leave-one-camera-out approach, which mirrors the realistic scenario where abundant data from various cameras is available for training, and experimentation occurs under diverse conditions. We demonstrate that our novel network and learning procedure alleviates the degradation in cross-camera distracted driver classification on the very recent 100-Driver dataset [4]. Experiments on the AUCDD-V1 [3], EZZ2021 [8], and SFD [9] datasets demonstrate the superior cross-dataset and cross-camera performance of our approach, highlighting its generalization capability. Our main contributions can be summarized as follows:

- A novel disentanglement module that makes features invariant to camera views, thereby enhancing driver action classification.
- Two triplet losses to aid in learning disentangled representations.
- A model that maintains low computational complexity while outperforming more advanced methods on four benchmark datasets.
- Feature analysis and ablation studies provide valuable insights on feature disentanglement and the impact of different design choices.

II. RELATED WORKS

Large-scale image recognition networks have proven effective in recognizing distracted driving. Abouelnaga *et al.* [10] employed a genetic-weighted ensemble of four CNNs, focusing on facial and hand features. Baheti *et al.* [11] optimized VGG16, reducing parameters and introducing L_2 regularization. Koay *et al.* [12] favored CNNs over Vision Transformers and proposed the OWIPA approach with pose estimation. Shaout *et al.* [13] used SqueezeNet for real-time distraction detection. However, in all these works cross-dataset performance was overlooked.

Specially designed models like MobileVGG with 2.2M parameters [14] advanced real-time detection. Nguyen *et al.* [15] developed a lightweight CNN with adaptive feature map extraction. Li *et al.* [16] proposed OLCMNet, an accurate lightweight network with an Octave-Like Convolution Mixed (OLCM) block. Liu *et al.* [17] used knowledge distillation and NAS, achieving high accuracy with 0.42M parameters. Mittal *et al.* [18] introduced CAT-CapsNet with impressive accuracies. Despite the reported improvements, fewer parameters may limit learning capabilities, especially in cross-dataset scenarios.

To mitigate the detrimental effects of background noise on recognition accuracy, Leekha *et al.* [19] proposed the use of an iterative graph-based foreground segmentation algorithm to separate the driver from the background, while Yang *et al.* [20] employed Gaussian Mixture Models (GMM) for body extraction. Qin *et al.* [21] introduced D-HCNN with 0.76M parameters, focusing on HOG features. Dey *et al.* [22] used

object detection for multiple ROIs, enhancing generalization. Behera *et al.* [23] proposed a contextual modeling approach that integrates posture and semantic context. They validated their approach using a self-annotated SFD test set and provided the first cross-validation results for the SFD dataset. Wang *et al.* [24] applied Fast-RCNN for DOA extraction. Keypoint-based approaches, like Li *et al.* [25] and Bera *et al.* [26], emphasized topological information. While effective, these methods demand extensive pre-processing, impacting real-time performance. Duan *et al.* [27] proposed S-Softmax classifier and a dynamic 2D supervision matrix for improving cross-dataset performance.

Researchers simplified training strategies for enhanced generalization. Masood *et al.* [28] used pretrained-weight VGG architectures for reduced training time. Li *et al.* [29] introduced Multi-Teacher Knowledge Distillation for lightweight models. Peng *et al.* [30] employed Few-Shot Learning for feature calibration. Contrastive and unsupervised methods, like Hu *et al.* [5] and Li *et al.* [31], focused on improved training strategies.

Compared to previous research, this paper tackles the issue of distracted drivers by enhancing model robustness without increasing computational demands. Notably, this is the first work to conduct comprehensive experiments using the leave-one-camera-out strategy, accurately reflecting real-world scenarios where the recognition model is trained under certain conditions and tested under different ones. This rigorous setup ensures our findings are both practical and applicable to real-world conditions.

III. THE PROPOSED DRIVER BEHAVIOR MONITORING NETWORK

A. Motivation

Image analysis-based DMSs encounter a significant challenge due to the variability in vehicle interior configurations, resulting in disparate camera viewpoints [4], [30]. Conventional supervised deep learning methods, often employing cross-entropy loss, struggle to develop robust representations capable of generalizing across different views. In these varied perspectives, where driver actions are observed, it becomes crucial to design supervised techniques that mitigate the drop in effectiveness when handling data acquired under conditions that differ from the training set.

Moreover, deploying these DMSs on devices with limited computational capacity necessitates the use of efficient and lightweight models, ensuring real-time predictions. Hence, robust solutions must be sought, incorporating deep learning models that respond to previous requirements.

B. Overview

Given the factors mentioned above, we present the Driver Behavior Monitoring Network (DBMNet), illustrated in Figure 1. This method encodes an RGB image by leveraging the lightweight CNN architecture detailed in [4] as its backbone. The proposed feature disentanglement module aims to prioritize action encoding over camera-view information. This is achieved by linearly combining view queries with features

estimated by the backbone. The resulting disentangled features are then forwarded to a linear layer for action classification. The model outputs two probability distributions: one for the driver's action categories and another for the viewpoint. The viewpoint distribution is used solely as an auxiliary task for the feature disentanglement module. The model is optimized through cross-entropy losses combined with triplet losses to assist in the learning of view-invariant action features.

C. The proposed model

a) *Backbone*: Our model consists of a GhostNet-v1.0 [32] as the backbone. Given an input image $\mathbf{X} \in \mathbb{R}^{C \times H \times W}$, the backbone f_b outputs a feature vector $\mathbf{f} = f_b(\mathbf{X}) \in \mathbb{R}^{1 \times D}$ as output, where D is the number of features.

b) *Feature disentanglement*: The output of the backbone is passed to the feature disentanglement module. This module consists of V learnable view queries $\mathbf{Q} \in \mathbb{R}^{D \times V}$, where V represents the number of views for the training samples. Through our learning process, we determine, for each view, which features are most relevant for characterizing the driver actions. The disentangled feature vector is obtained as a weighted combination of the view queries with the feature vector \mathbf{f} , determined by the backbone. The weighting, denoted as \mathbf{w} , is computed based on which view or views the test sample most closely resembles. In practice, estimating the disentangled features is carried out as follows:

$$\hat{\mathbf{f}} = \mathbf{w} \times \mathbf{f}, \quad (1)$$

$$\text{with } \mathbf{w} = \mathbf{p}_v \cdot \mathbf{Q}, \quad (2)$$

where \mathbf{p}_v is the probability distribution over V views that is estimated by the view classifier.

c) *Classifiers*: The model consists of two classifiers, namely the Action classifier for categorizing the action performed by the driver and the View classifier for the estimation of the camera viewpoint. The Action classifier takes as input the disentangled feature vector $\hat{\mathbf{f}}$ and outputs the probability distribution over the A action classes, $\mathbf{p}_a \in \mathbb{R}^{1 \times A}$, as follows:

$$\mathbf{p}_a = (\mathbf{W}_a \hat{\mathbf{f}}) + \mathbf{b}_a, \quad (3)$$

where $\mathbf{W}_a \in \mathbb{R}^{D \times A}$ and $\mathbf{b}_a \in \mathbb{R}^{1 \times A}$ are the weights and bias of the fully-connected head for action classification.

Instead, the View classifier processes the feature vector \mathbf{f} produced directly from the backbone to produce the probability distribution, \mathbf{p}_v , on the V views as follows:

$$\mathbf{p}_v = (\mathbf{W}_v \mathbf{f}) + \mathbf{b}_v. \quad (4)$$

In the previous equations, $\mathbf{W}_v \in \mathbb{R}^{D \times V}$ and $\mathbf{b}_v \in \mathbb{R}^{1 \times V}$ are the weights and bias of the fully-connected layer for view classification.

D. Training procedure

a) *Training data input*: During training, our model processes batches of image triplets with an approach similar to that of Siddiqui *et al.* [33]. Each triplet comprises an anchor image, denoted as a , which portrays a driver's action from a specific viewpoint. Another image in the triplet, referred to

as sv (same view), displays a different action captured from the identical viewpoint as a . Finally, we include an image of the same action as a , but captured from a distinct viewpoint, denoted as sa (same action). We construct these triplets to provide both positive and negative samples for our supervised contrastive learning, which will be presented in the following section. By supplying both positive and negative samples, the model can develop a comprehensive understanding of the discriminative characteristics within each action or viewpoint category through sample comparisons. This methodology diverges from the learning-by-classification approach, wherein the loss function solely penalizes classification errors without explicitly promoting intraclass compactness and interclass separation [34].

b) *Loss function*: Our DBMNet is trained through a composite loss function that is defined as follows:

$$\mathcal{L} = \mathcal{L}_{ace} + \mathcal{L}_{vce} + \mathcal{L}_{ac} + \mathcal{L}_{vc}. \quad (5)$$

In the previous loss, there are two cross-entropy losses mainly dedicated to the optimization of linear layers for view (\mathcal{L}_{vce}) and action (\mathcal{L}_{ace}) categorization. Cross-entropy losses are only applied to the anchor image in this way:

$$\mathcal{L}_{vce} = - \sum_{m=1}^V y_v^{(m)} \log(p_v^{(m)}), \quad (6)$$

$$\mathcal{L}_{ace} = - \sum_{m=1}^A y_a^{(m)} \log(p_a^{(m)}). \quad (7)$$

with A and V being the number of actions and the number of views, respectively. $p_a^{(m)}$ is the probability of the m -th category with ground-truth $y_a^{(m)}$ for the action of the anchor sample, while $p_v^{(m)}$ is the probability of the m -th category with ground-truth $y_v^{(m)}$ for the anchor sample viewpoint.

The previous two cross-entropy losses are complemented by two opposite triplet losses. Both losses use the same triplet construction previously defined. The difference lies in the role assumed by sv and sa in each loss.

In the action triplet loss (Eq. 8) the objective is to learn features for action encoding that are invariant regardless of the viewpoint. Hence, sa serves as the positive sample, whereas sv serves as the negative sample. This choice has the purpose of bringing closer the representations of sa and a which have the same action. Conversely, the distance between the representations of a and sv that depict a different action from the same point of view is instead maximized:

$$\mathcal{L}_{ac} = \sum_{n=1}^N [\delta + \mathcal{D}(\hat{\mathbf{f}}_a, \hat{\mathbf{f}}_{sa}) - \mathcal{D}(\hat{\mathbf{f}}_a, \hat{\mathbf{f}}_{sv})], \quad (8)$$

where $\hat{\mathbf{f}}_a$, $\hat{\mathbf{f}}_{sa}$, and $\hat{\mathbf{f}}_{sv}$ denote the disentangled feature outputs from the a , sa , and sv images, respectively. $\mathcal{D}(\cdot, \cdot)$ is the pairwise Euclidean distance function, and δ is a margin parameter. It is expected that the learned disentangled features exhibit view-invariance, as they are encouraged to be as similar as possible when derived from two different images depicting the same action regardless of the viewpoint from which they were acquired.

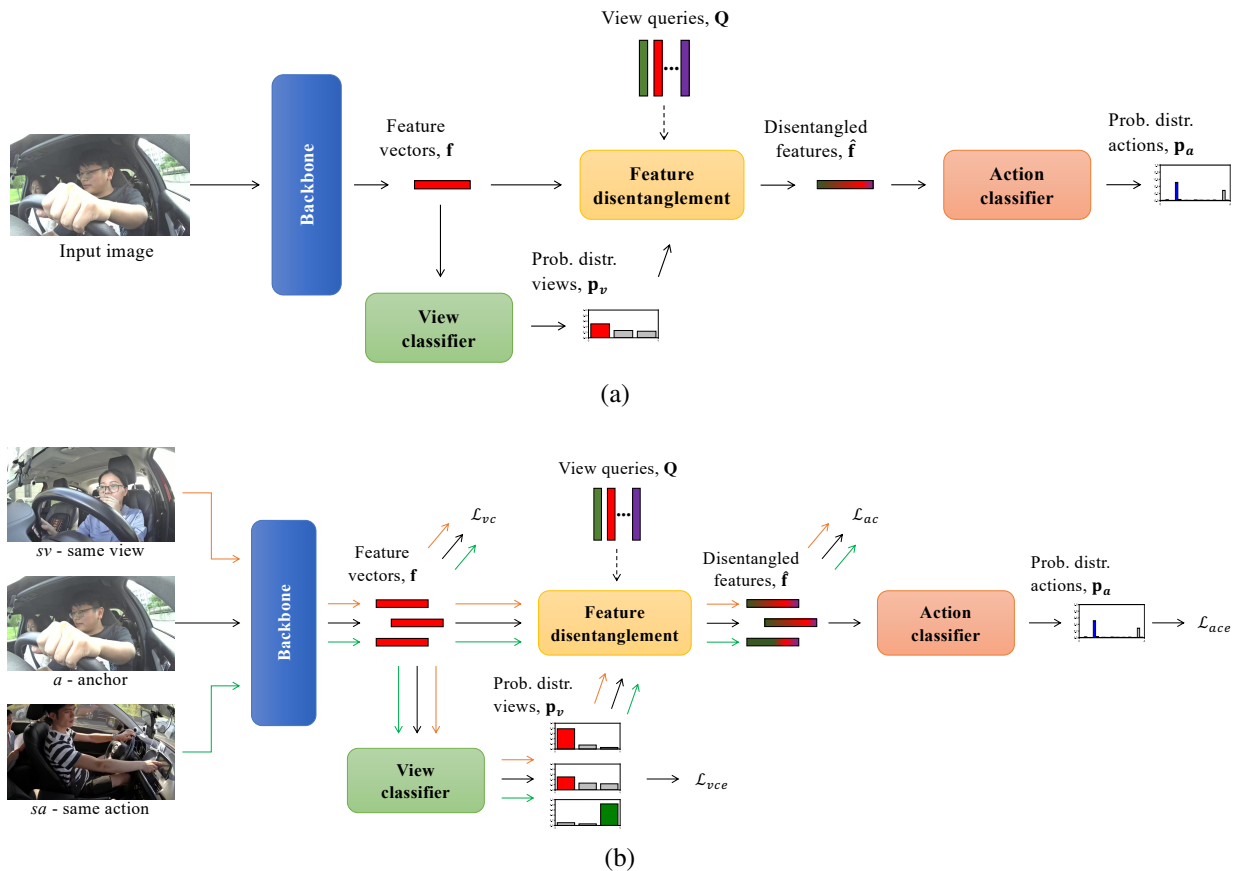


Fig. 1. The *DBMNet* pipeline. At inference time (a), the backbone encodes an RGB image into a feature vector \mathbf{f} . The feature disentanglement module then refines these features to discard view-related information while retaining action-related details using view queries, \mathbf{Q} , together with the probability distribution over the views. The resulting features $\hat{\mathbf{f}}$ are mapped into a driver action by the action classifier. During training (b), alongside the cross-entropy loss for action and view prediction (respectively, \mathcal{L}_{ace} and \mathcal{L}_{vce}), we employ the triplet loss (\mathcal{L}_{ac} and \mathcal{L}_{vc}). This triplet loss helps to learn distinct action and view representations by processing three input images: an anchor image a , an image sv depicting the same view but different action as a , and an image sa with the same action but from a different view as a .

For the view triplet loss, positive and negative samples are reversed:

$$\mathcal{L}_{vc} = \sum_{n=1}^N [\delta + \mathcal{D}(\mathbf{f}_a, \mathbf{f}_{sv}) - \mathcal{D}(\mathbf{f}_a, \mathbf{f}_{sa})]. \quad (9)$$

In this way, the feature disentanglement module, particularly the view queries, learns to generate similar features for images acquired from the same viewpoint, regardless of the action being performed. Since our primary goal is to enhance multi-view driver action recognition, training our model to distinguish action-relevant features from view-relevant features in this manner provides cleaner and more accurate action representations that are robust to changes in the camera viewpoint.

IV. EXPERIMENTS

In this section, we present the datasets used in the experiments, describe the experimental setup, and discuss the results of our extensive experimentation.

A. Dataset

We conduct extensive experiments on 100-Driver [4]. The 100-Driver dataset comprises 470,000 images illustrating 100

drivers engaged in 22 distinct actions during driving sessions. These actions include 21 distracted behaviors and one instance of normal driving (see Table I for the list of all actions).

The driving sessions were recorded in both daytime and nighttime in five different vehicles, comprising two sedans, two SUVs, and one van. Within each vehicle, four cameras were strategically placed - on the left front, right front, and right side of the drivers. This arrangement served dual purposes. Firstly, having a dataset with multiple cameras aids in developing more robust models that can account for variations in camera perspectives, thus evaluating the models' generalization across different cameras. Secondly, the multi-camera dataset offers an opportunity to enhance system performance by considering the content captured from multiple camera angles. Figure 2 reports samples from the four cameras in both day and night times.

We also perform cross-dataset evaluation on the AUCDD-V1 [3], EZZ2021 [8] and SFD [9] datasets. Image for these datasets are annotated based on 10 different driver actions: Safe/Normal driving, Texting (right), Talking with cellphone (right), Texting (left), Talking with cellphone (left), Adjusting radio, Drinking, Reaching behind, Hair and makeup, Talking to passenger. AUCDD-V1 consists of 12,978 training images

TABLE I
THE LIST OF DRIVER ACTIONS IN THE 100-DRIVER DATASET [4].

No.	Action	No.	Action	No.	Action	No.	Action
0	Normal driving	6	Texting (right)	12	Smoking (left)	18	Operating GPS
1	Sleeping	7	Hair / makeup	13	Smoking (right)	19	Reaching behind
2	Yawning	8	Looking left	14	Smoking (mouth)	20	Hands off the steering wheel
3	Talk with cellphone (left)	9	Looking right	15	Drinking / Eating (left)	21	Talking to passenger
4	Talk with cellphone (right)	10	Looking up	16	Drinking / Eating (right)		
5	Texting (left)	11	Looking down	17	Adjusting radio		



Fig. 2. Sample images showcasing a driver engaged in both safe and distracted driving behavior, taken from the 100-Driver dataset [4]. The images are captured with four cameras installed in the same vehicle in both daytime (D1, D2, D3 and D4) and nighttime (N1, N2, N3 and N4) contexts.

and 4,331 test images. We evaluate model performance only on the test images. In the EZZ2021 dataset, 9 drivers are depicted performing the previous actions. Since a data split is not provided, all images are used for testing. The SFD dataset, used in a Kaggle competition, comprises 22,424 training images and 79,726 test images. The training images are labeled with 10 class labels, while the test images are not labeled. Therefore, only the training set is used for evaluation.

B. Experimental Setup

1) *Evaluation*: We run experiments in a cross-camera setup which is implemented by applying the leave-one-camera-out protocol on the 100-Driver dataset. Given that the cameras were placed at 4 different points, for each round 3 cameras are used for training and the other one for evaluation. Our train-val-test splits are obtained by aggregating the splits defined in [4] according to our protocol. We measure method performance in terms of Top-1 and Top-5 accuracy.

2) *Backbones*: We select three efficient backbone models to assess the impact of varying parameter counts on our method including GhostNet-v1.0 [32], MobileNetV3-S [35], and SqueezeNet-v1.1 [36].

3) *Implementation details*: Our experiments are performed on a computer featuring an Intel i7-8700 CPU @3.20GHz and an NVIDIA GeForce GTX 1070 Ti. The operating system is Ubuntu 22.04, and the framework is PyTorch 2.0.1. We utilize the SGD optimizer with a momentum of 0.9 and a weight decay equal to 5×10^{-4} . The batch size is set to 64. The GhostNet-v1.0 backbone is pretrained on ImageNet. The view

queries are randomly initialized by sampling from a normal distribution with mean equal to 0 and variance 1.

The learning rate is initialized to 0.01 and reduced by a factor of 10 at 10 and 30 epochs. The inputs are first resized to 224×224 pixels. We then use random rotation in the range $[-30^\circ, 30^\circ]$, random perspective, random color transformations in terms of contrast, saturation and hue, Gaussian blur, and random erasing [37] for data augmentation. Training is performed for a total of 50 epochs. The best-performing epoch on the validation set in terms of Top-1 accuracy is then chosen for evaluation on the test data. The margin δ of triplet losses is empirically set to 1. Performance metrics are Top-1 and Top-5 accuracy.

C. Results

1) *Ablation study*: In this section we present the results detailing the contribution of the key components within the proposed model. Specifically, we compare three different efficient backbones and we assess the contribution of contrastive learning, the influence of the disentanglement module, and finally, the effect of their combined integration.

a) *Model backbone*: Table II reports the comparison of the three model architectures in terms of number of parameters and number of floating point operations per second (FLOPS). The GhostNet-v1.0 model has 5.2 million parameters and 0.16 GFlops, which indicates a moderate computational complexity with a relatively higher number of parameters compared to the other models. On the other hand, the MobileNetV3-S model, demonstrates a significantly lower number of parameters at 2.5 million and the lowest computational complexity with

TABLE II
COMPARISON OF THE THREE MODELS EXPLOITED AS BACKBONE OF THE
PROPOSED METHOD IN TERMS OF NUMBER OF PARAMETERS AND
COMPUTATIONAL COMPLEXITY.

Model	Params	GFlops
GhostNet-v1.0 [32]	5.2M	0.16
MobileNetV3-S [35]	2.5M	0.06
SqueezeNet-v1.1 [36]	1.2M	0.35

0.06 GFlops. Finally, the SqueezeNet-v1.1 model features the smallest number of parameters at 1.2 million but has the highest computational complexity among the three, with 0.35 GFlops.

The results reported in Table III reveal notable performance differences among the considered backbones in the leave-one-camera-out experiments. GhostNet consistently demonstrates superior performance across most daytime and nighttime scenarios. For instance, it achieves the highest Top-1 accuracy of 62.51% and Top-5 accuracy of 93.75% when evaluating D2. This suggests that GhostNet is particularly effective in handling variations across different camera configurations. MobileNetV3 also performs well, especially during nighttime acquisitions, where it shows competitive results in some scenarios. For example, it achieves a Top-1 accuracy of 33.18% for N1 and 47.75% for N2, indicating its robustness in lower light conditions. However, its overall performance remains slightly lower than GhostNet’s across most evaluations. SqueezeNet, on the other hand, consistently underperforms compared to GhostNet and MobileNetV3. It struggles particularly in more challenging scenarios such as D4 and N4, where it records a notably low Top-1 accuracy of 7.91% and 4.22%, respectively. This highlights potential limitations of SqueezeNet in handling diverse and complex data conditions.

b) Contrastive learning contribution: This version of DBMNet consists of the Backbone, and the two classifiers, namely the View and Action classifiers. The model is optimized by combining cross-entropy losses and triplet losses for each task. The results for this version are reported in the first row of Table IV. As it is possible to see, the lack of the feature disentanglement module compared to the full solution (the results of which are shown in the last row of the table) negatively impacts the results. On average, there is a loss of 5.42% and 4.05% on Top-1 and Top-5 accuracy, respectively. The highest gap corresponding to 13.54% of Top-1 accuracy is registered for Camera 3.

c) Feature disentanglement module contribution: In this experiment, the architecture of DBMNet remains unchanged. The difference with the complete version lies solely in the choice of loss function utilized for model optimization. Specifically, we incorporate only the two cross-entropy losses. The outcomes for this variant are depicted in the second row of Table IV. We emphasize that also the performance of this solution is inferior to that of the full version of DBMNet. Notably, there is a 6.94% drop in Top-1 and 8.79% drop in Top-5. More significantly, these results are even lower than those achieved with Contrastive learning alone. Consequently, it is evident that while the Feature Disentanglement module

offers benefits to DBMNet, the use of Contrastive learning yields even greater advantages.

d) Full solution analysis: DBMNet capitalizes on the advantages offered by both the Feature disentanglement module and Contrastive learning, as outlined in the previous sections. Our focus is on another important aspect of our method in this section. Given that DBMNet performs feature disentanglement by highlighting the features for the driver’s actions based on the view that is most similar to the test view, it is imperative to ensure the effectiveness of view classification. We register an average performance for the four rounds of leave-one-camera-out equal to 98.54% on the validation set of Driver-100. This means that the view classification is accurate and should be able to correctly guide the choice of the view queries.

2) Comparison with other methods: In this section, we compare the results achieved by our DBMNet with those of four recent methods, namely Duan *et al.* [27], GhostNet [4], Hu *et al.* [5], and OLCMNet [16]. It is worth noting that Duan *et al.* trained a GhostNet-v1.0 by exploiting their proposed S-Softmax classifier for improving model robustness. GhostNet is the same architecture used in our method as the backbone, and unlike our method, it is trained exclusively through cross-entropy loss optimization for driver action classification. Hu *et al.* [5] trained a ResNet-18 using a compound loss, which includes the proposed Clustering Supervised Contrastive Loss (C-SCL) for improving action representations, along with the cross-entropy loss used for the classification head. For a fair comparison with our DBMNet, we replaced the ResNet18 architecture with our GhostNet-v1.0. Finally, OLCMNet is a lightweight network with an OLCM block to improve model effectiveness.

Table V reports the results for each round of our leave-one-camera-out protocol. According to the results, several considerations can be made. First, the worst result obtained by our model is for the D4 camera, Top-1 accuracy 11.29%, compared with the best result obtained for D2 of 62.51% Top-1 accuracy. This result was expected since the framing of the driver is very different from the other three cameras (see Figure 2 for a better understanding). Second, the cameras are ranked in descending order based on their Top-1 performance as follows: D2, D3, D1, and D4. This ranking serves as a valuable indicator of the viewpoints offering superior driver visibility, thereby guiding the optimal placement of cameras. Third, our DBMNet demonstrates superior performance compared to the other two methods with an average improvement of 9% across all four cameras. In particular, the most significant disparity is observed against GhostNet, where DBMNet achieves a remarkable 17.20% increase in Top-1 accuracy and a 16.44% increase in Top-5 accuracy on camera D3. Still, on camera D3, DBMNet exhibits the largest performance improvement over Hu *et al.*, with an improvement of 7.32% and 5.87% in Top-1 and Top-5 accuracy, respectively.

Figure 3 shows the confusion matrices for each cross-camera configuration. For the daytime subset we can the following observations. Confirming that the best performance is obtained for D2 and D3, there is a prominent diagonal in the respective confusion matrices. The confusion matrix for D1 shows a high bias in the class “Hair / Makeup” (#7). Many

TABLE III

COMPARISON OF THE CONSIDERED BACKBONES IN TERMS OF TOP-1 AND TOP-5 (%) ACCURACY FOR OUR LEAVE-ONE-CAMERA-OUT EXPERIMENTS. D AND N INDICATE ACQUISITIONS DURING THE DAYTIME AND NIGHTTIME, RESPECTIVELY. THE NUMBER FOLLOWING THE D OR N INDICATES THE CAMERA ID. THE NAMES ON THE LEFT SIDE OF THE ARROW REFER TO THE TRAINING CAMERAS, WHILE THE NAME ON THE RIGHT SIDE OF THE ARROW REFERS TO THE EVALUATED CAMERA.

	D{2,3,4} → D1		D{1,3,4} → D2		D{1,2,4} → D3		D{1,2,3} → D4		N{2,3,4} → N1		N{1,3,4} → N2		N{1,2,4} → N3		N{1,2,3} → N4	
	Top-1	Top-5														
GhostNet	32.37	72.55	62.51	93.75	50.99	82.56	11.29	39.31	31.95	69.09	49.19	83.79	19.39	55.85	8.63	29.69
MobileNetV3	18.72	63.19	53.48	85.45	37.23	72.22	9.10	38.60	33.18	70.21	47.75	81.78	18.37	49.68	5.30	24.25
SqueezeNet	15.72	47.01	35.62	82.39	39.11	72.90	7.91	32.54	33.02	69.38	45.99	78.42	15.84	46.27	4.22	21.06

TABLE IV

ABLATION EXPERIMENTS ABOUT FEATURE DISENTANGLEMENT AND CONTRASTIVE LEARNING, USING TOP-1 AND TOP-5 (%) ACCURACY FOR LEAVE-ONE-CAMERA-OUT EXPERIMENTS.

Feat. disent.	Contr. learn.	{D2,D3,D4} → D1		{D1,D3,D4} → D2		{D1,D2,D4} → D3		{D1,D2,D3} → D4	
		Top-1	Top-5	Top-1	Top-5	Top-1	Top-5	Top-1	Top-5
	✓	28.99	70.00	61.05	91.58	37.45	76.32	7.99	34.06
✓		28.22	66.15	58.13	87.47	34.27	65.87	8.80	33.51
✓	✓	32.37	72.55	62.51	93.75	50.99	82.56	11.29	39.31

TABLE V

TOP-1 AND TOP-5 (%) ACCURACY FOR OUR LEAVE-ONE-CAMERA-OUT EXPERIMENTS. D INDICATES ACQUISITIONS DURING THE DAYTIME. THE NUMBER FOLLOWING THE D INDICATES THE CAMERA ID. THE NAMES ON THE LEFT SIDE OF THE ARROW REFER TO THE TRAINING CAMERAS, WHILE THE NAME ON THE RIGHT SIDE OF THE ARROW REFERS TO THE EVALUATED CAMERA.

	D{2,3,4} → D1		D{1,3,4} → D2		D{1,2,4} → D3		D{1,2,3} → D4		N{2,3,4} → N1		N{1,3,4} → N2		N{1,2,4} → N3		N{1,2,3} → N4	
	Top-1	Top-5														
Duan <i>et al.</i> [27]	8.86	40.92	14.40	47.39	12.61	42.46	7.25	30.17	13.78	43.53	11.62	43.09	5.85	25.83	4.82	27.80
GhostNet [4]	21.54	64.96	57.89	85.46	33.79	66.12	8.85	32.35	26.43	61.16	47.12	80.90	17.37	48.24	4.89	23.97
Hu <i>et al.</i> [5]	27.39	70.20	59.70	89.48	43.67	76.69	5.45	29.17	29.67	62.03	47.50	80.27	17.26	45.83	4.02	25.81
OLCMNet [16]	20.51	68.97	55.71	81.35	34.03	68.91	8.48	30.17	25.50	63.51	40.64	76.81	12.77	30.91	5.54	23.93
DBMNet (ours)	32.37	72.55	62.51	93.75	50.99	82.56	11.29	39.31	31.95	69.09	49.19	83.79	19.39	55.85	8.63	29.69

of the test samples are wrongly categorized with this class. An analysis of the distribution of the samples per category, however, excludes the presence of an imbalance in sample cardinality that could favor any specific category. Therefore, the negative results can only be attributed to the poor generalization ability of the model on this viewpoint. In the case of D4, “Looking to the left” (#8) and “Reaching behind” (#19) consistently emerge as the most frequently predicted categories for the test samples, even when predictions are incorrect. With an accuracy rate of 53.00%, the class “Drinking / Eating (right)” stands as the second most accurately classified category for this camera. In general, for all daytime cameras, the “Looking Left” (#8) class is recognized with the highest rate. Confusion matrices for the nighttime subset reflect the poor performance, with only N1 and N2 presenting a discernible diagonal. The highest performance for N1 is observed in the “Reaching behind” (#19) class with 77% accuracy and the “Hair / Makeup” (#7) class with 71% accuracy. For N2, several classes achieve accuracy higher than or equal to 70%, namely “Talk with cellphone (left)” (#3), “Talk with cellphone (right)” (#4), “Looking Left” (#8), “Looking up” (#10), and “Operating GPS” (#18). In the case of N3, the model shows a high concentration of false positives for the “Normal driving” (#0) and “Reaching behind” (#19) classes. For N4, “Talk with cellphone (right)” (#4) and “Hair / Makeup” (#7) classes are recognized with accuracies of 44% and 54%, respectively. The lower performance for N4 might be due to its significant difference from the other views, making it challenging to

recognize actions accurately, with only these two actions being relatively easier to identify.

3) *Cross-dataset results*: Since the camera configuration for AUCDD-V1, EZZ2021, and SFD is very similar to that of camera D4 in the 100-Driver dataset (see Figure 4), we perform inference on these three datasets using the model trained on images acquired from cameras D1, D2, and D3. Thus, we can state that the current setup constitutes a cross-camera and cross-dataset experiment. The experimental results shown in Table VI highlight the performance of different models on the D4 test set of 100-Driver and the AUCDD-V1, EZZ2021, and SFD datasets. It is evident from the results that DBMNet, our proposed model, outperforms the other models across most metrics. Specifically, DBMNet achieves the highest Top-1 accuracy on the D4 test set of 100-Driver (11.29%), AUCDD-V1 (7.71%), EZZ2021 (10.51%), and SFD (9.86%). Similarly, for Top-5 accuracy, DBMNet also shows superior performance on the D4 test set of 100-Driver (39.31%) and SFD (38.62%). In contrast, GhostNet, Hu *et al.*, and Duan *et al.* models exhibit lower Top-1 and Top-5 accuracies in most cases. For instance, GhostNet shows a Top-1 accuracy of 8.85% on the D4 test set of 100-Driver, which is lower than that of DBMNet. Similarly, the Top-5 accuracy of Hu *et al.* on EZZ2021 is only 21.53%, significantly less than the 34.09% achieved by DBMNet. Duan *et al.*'s model performs comparatively better than GhostNet and Hu *et al.*, but still falls short of DBMNet, particularly in the SFD dataset where DBMNet achieves a Top-1 accuracy

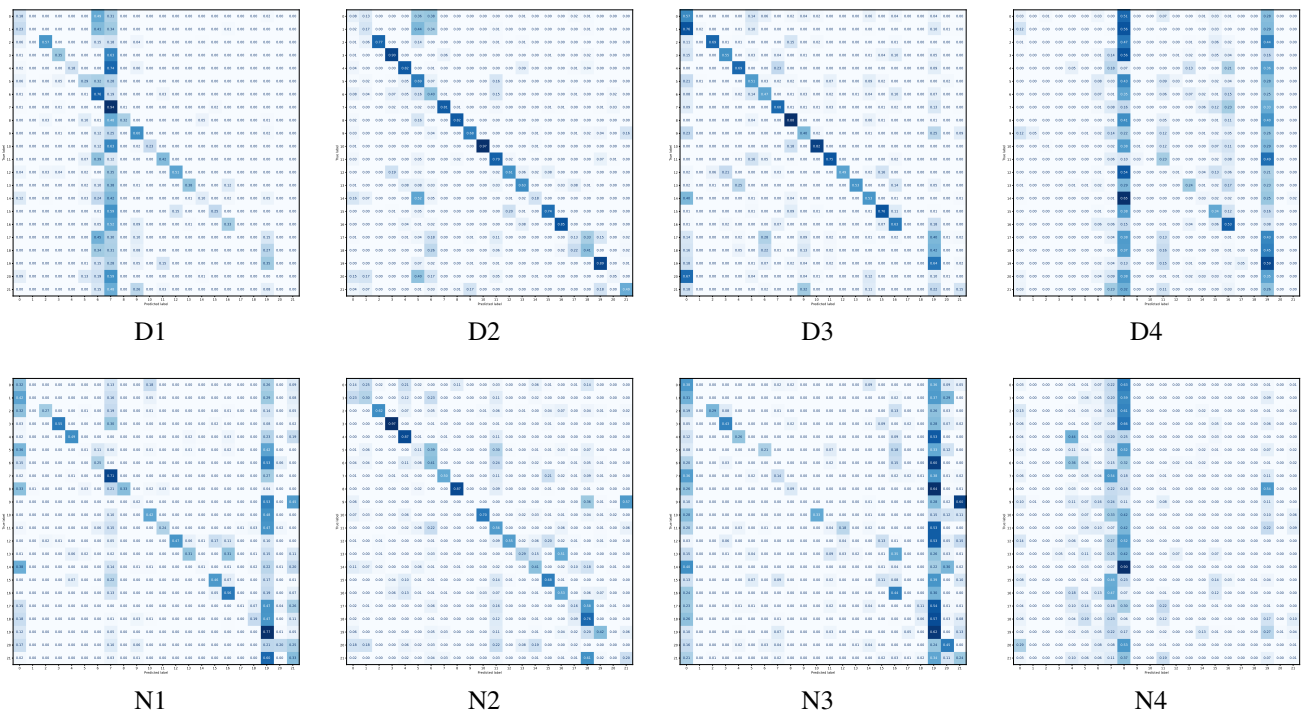


Fig. 3. Confusion matrix for each cross-camera configuration (best viewed zoom in).



Fig. 4. Sample images showing consistency in framing in the 100-Driver (using the D4 camera) [4], AUCDD-V1 [3], EZZ2021 [8] and SFD [9] datasets.

of 9.86% and a Top-5 accuracy of 38.62%. These results indicate that DBMNet’s training on the combination of D1, D2, and D3 cameras of the 100-Driver dataset provides a more robust model for cross-camera and cross-dataset applications, demonstrating improved generalization and higher accuracy across diverse datasets.

4) *Analysis:* In this section, we conduct an analysis of features to support our claim of disentangled features. To this end, we qualitatively evaluate how the features before and after disentanglement module separate in the embedding space and quantitatively estimate the capacity of discriminating viewpoints before and after feature disentanglement. Practically, we extract feature vectors before and after the View disentanglement module, namely \mathbf{f} and $\hat{\mathbf{f}}$, for both training and validation images. We chose validation images because the camera view categories overlap with those of the training set, unlike those of the test set. Figure 5 illustrates the features of the validation set for the image subset D1, D2, D3 using t-Distributed Stochastic Neighbor Embedding (t-SNE). The colors represent different driver action classes. As depicted, the \mathbf{f} -features separate into small, distinct clusters, even for the same action class, likely due to the actions being captured by different cameras. In contrast, the $\hat{\mathbf{f}}$ -features form larger clusters that more effectively distinguish between different

actions regardless of the camera used, thereby demonstrating the effectiveness of the feature disentanglement module. We then exploit a Minimum Distance Classifier (MDC) to classify camera viewpoints. Specifically, we train an MDC classifier on \mathbf{f} feature vectors, referred as $\text{MDC}_{\mathbf{f}}$, and another MDC classifier on $\hat{\mathbf{f}}$ feature vectors, labeled as $\text{MDC}_{\hat{\mathbf{f}}}$. Finally, we classify \mathbf{f} validation samples with $\text{MDC}_{\mathbf{f}}$ and $\hat{\mathbf{f}}$ validation samples with $\text{MDC}_{\hat{\mathbf{f}}}$. Results are reported in Table VII. As can be seen, the accuracy of view classification undergoes a drop after feature disentanglement. On average, there is a decrease of 21.07%, with the most significant drop for D4 at 34.08% and the least pronounced for Camera 1 and 2, around 11.05%. This means that view information is discarded in favor of a better ability to discriminate drivers’ actions.

V. CONCLUSIONS

Driver Monitoring Systems (DMSs) need to be robust to changes in vehicle configuration and camera positions. In this paper, we introduced DBMNet, a novel network designed for distracted driver classification, ensuring consistent performance regardless of camera placement. Given that DMSs operate on embedded devices with constrained computational resources, our model exploits GhostNet, a lightweight CNN, as the backbone. We improved the invariance to the camera

TABLE VI
TOP-1 AND TOP-5 ACCURACY (%) ON THE D4 TEST SET OF 100-DRIVER, AND THE AUCDD-V1, EZZ2021 AND SFD DATASETS FOR THE MODEL TRAINED ON THE COMBINATION OF D1, D2 AND D3 CAMERAS OF THE 100-DRIVER DATASET.

	Top-1				Top-5			
	100-Driver	AUCDD-V1	EZZ2021	SFD	100-Driver	AUCDD-V1	EZZ2021	SFD
Duan <i>et al.</i> [27]	7.25	6.42	8.33	9.31	30.17	30.15	30.88	28.87
GhostNet [4]	8.85	6.79	8.08	4.59	32.35	29.62	31.80	23.20
Hu <i>et al.</i> [5]	5.45	5.75	8.10	4.84	29.17	27.61	21.53	24.31
OLCMNet [16]	8.48	5.56	9.94	4.96	30.17	28.09	27.62	25.11
DBMNet (ours)	11.29	7.71	10.51	9.86	39.31	30.80	34.09	38.62

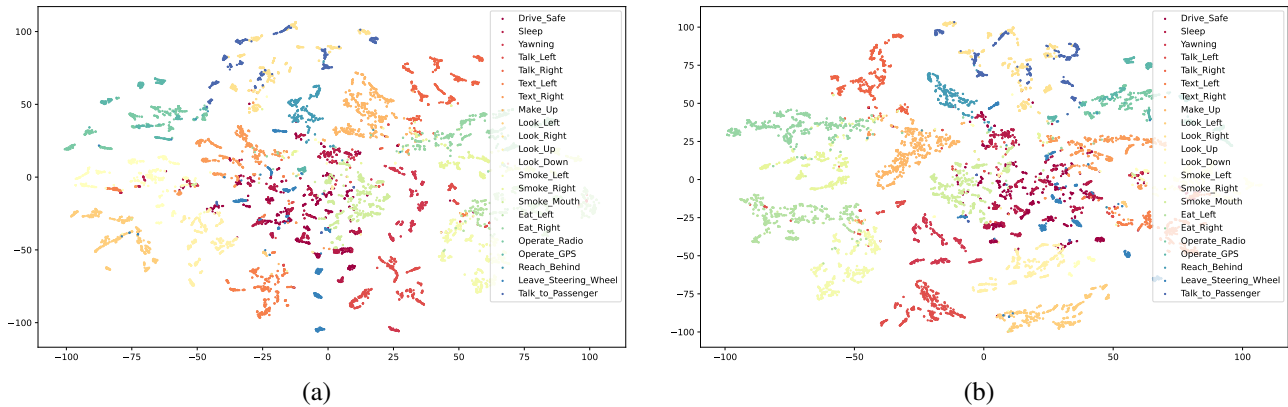


Fig. 5. Analysis of features learned by our DBMNet using t-Distributed Stochastic Neighbor Embedding (t-SNE). Using the model trained on the {D1,D2,D3} images, we report for the validation images (a) the feature vectors \mathbf{f} extracted by the backbone, and (b) the feature vectors $\hat{\mathbf{f}}$ after the disentanglement module.

TABLE VII
RESULTS OF AN MDC ON THE VALIDATION SET FOR THE DIFFERENT CROSS-CAMERA SETUPS.

	View cls acc. ($\mathbf{f} \rightarrow \hat{\mathbf{f}}$)
{D2,D3,D4} \rightarrow D1	31.61 \rightarrow 19.52
{D1,D3,D4} \rightarrow D2	32.06 \rightarrow 20.95
{D1,D2,D4} \rightarrow D3	44.86 \rightarrow 19.87
{D1,D2,D3} \rightarrow D4	70.83 \rightarrow 34.75

view of the representation using a feature disentanglement module. In addition, we employed a supervised contrastive learning approach to increase consistency between intra-class representations and differentiate inter-class representations. Experimental results on the 100-Driver dataset demonstrated the effectiveness of the proposed model with an increment on average of 9% in Top-1 accuracy with respect to state-of-the-art methods. Through the analysis of features both before and after the feature disentanglement module, we determined that the objective of discarding view information is accomplished.

Some limitations are worth noting. Given the inherent complexity of the task, the accuracy results obtained are modest, indicating a need for further refinement to enhance the generalization capacity of our DBMNet. This requirement is particularly pronounced due to the low accuracy observed in the “Normal driving” class, which often gets confused with other distraction classes. Additionally, the inference time on our computational setup stands at 1.15×10^{-2} seconds, which remains relatively high for ensuring timely detection of driver distraction, hindering the implementation of effective safety systems.

Considering these identified limitations, as part of future endeavors, we aim to explore lighter backbones beyond GhostNet utilized in our experiments. This exploration aims to minimize the inference time while maintaining performance. Furthermore, we plan to investigate few-shot learning methods to calibrate the model to novel viewpoints, leveraging a limited number of training samples. These strategies are pivotal for addressing the current constraints and advancing the effectiveness of DMSs.

ACKNOWLEDGMENT

Financial support from ICSC – Centro Nazionale di Ricerca in High Performance Computing, Big Data and Quantum Computing, funded by European Union – NextGenerationEU.

REFERENCES

- [1] W. H. Organization, “Global status report on road safety 2023,” *World Health Organization*, 2023.
- [2] Y. Choi, S. I. Han, S.-H. Kong, and H. Ko, “Driver status monitoring systems for smart vehicles using physiological sensors: A safety enhancement system from automobile manufacturers,” *IEEE Signal Processing Magazine*, vol. 33, no. 6, pp. 22–34, 2016.
- [3] H. M. Eraqi, Y. Abouelnaga, M. H. Saad, M. N. Moustafa *et al.*, “Driver distraction identification with an ensemble of convolutional neural networks,” *Journal of Advanced Transportation*, vol. 2019, 2019.
- [4] J. Wang, W. Li, F. Li, J. Zhang, Z. Wu, Z. Zhong, and N. Sebe, “100-driver: A large-scale, diverse dataset for distracted driver classification,” *IEEE Trans. Intell. Transport. Syst.*, 2023.
- [5] Z. Hu, Y. Xing, W. Gu, D. Cao, and C. Lv, “Driver anomaly quantification for intelligent vehicles: A contrastive learning approach with representation clustering,” *IEEE Trans. Intell. Veh.*, vol. 8, no. 1, pp. 37–47, 2023.

- [6] S. Bianco, L. Celona, G. D. Gallo, and P. Napolitano, "A platform for multi-modal driver behaviour data collection," in *International Conference on Consumer Electronics-Berlin*. IEEE, 2023, pp. 112–116.
- [7] A. Behera and A. H. Keidel, "Latent Body-Pose guided DenseNet for Recognizing Driver's Fine-grained Secondary Activities," in *IEEE Int. Conf. Adv. Video Signal-Based Surveill. (AVSS)*. IEEE, 2018, pp. 1–6.
- [8] A. Ezzouhri, Z. Charouh, M. Ghogho, and Z. Guennoun, "Robust deep learning-based driver distraction detection and classification," *IEEE Access*, vol. 9, pp. 168 080–168 092, 2021.
- [9] "Distracted driver detection competition," 2020. [Online]. Available: <https://www.kaggle.com/c/state-farm-distracted-driver-detection>
- [10] Y. Abouelnaga, H. M. Eraqi, and M. N. Moustafa, "Real-time distracted driver posture classification," in *Proc. Conf. Neural Inf. Process. Syst. (NIPS)*, 2018, pp. 1–8.
- [11] B. Baheti, S. Gajre, and S. Talbar, "Detection of distracted driver using convolutional neural network," in *CVPRW*. IEEE, 2018, pp. 1145–1151.
- [12] H. V. Koay, J. H. Chuah, and C.-O. Chow, "Convolutional neural network or vision transformer? benchmarking various machine learning models for distracted driver detection," in *IEEE Reg. 10 Annu. Int. Conf. Proc. TENCON*. IEEE, 2021, pp. 417–422.
- [13] A. Shaout, B. Roytburd, and L. A. Sanchez-Perez, "An embedded deep learning computer vision method for driver distraction detection," in *Int. Arab Conf. Inf. Technol., (ACIT)*. IEEE, 2021, pp. 1–7.
- [14] B. Baheti, S. Talbar, and S. Gajre, "Towards computationally efficient and realtime distracted driver detection with mobilevgg network," *IEEE Trans. Intell. Veh.*, vol. 5, no. 4, pp. 565–574, 2020.
- [15] Duy-Linh Nguyen, M. D. Putro, and K.-H. Jo, "Driver behaviors recognizer based on light-weight convolutional neural network architecture and attention mechanism," *IEEE Access*, vol. 10, pp. 71 019–71 029, 2022.
- [16] P. Li, Y. Yang, R. Grosu, G. Wang, R. Li, Y. Wu, and Z. Huang, "Driver distraction detection using octave-like convolutional neural network," *IEEE Trans. Intell. Transport. Syst.*, vol. 23, no. 7, pp. 8823–8833, 2022.
- [17] D. Liu, T. Yamasaki, Y. Wang, K. Mase, and J. Kato, "Toward extremely lightweight distracted driver recognition with distillation-based neural architecture search and knowledge transfer," *IEEE Trans. Intell. Transport. Syst.*, vol. 24, no. 1, pp. 764–777, 2023.
- [18] H. Mittal and B. Verma, "CAT-CapsNet: A convolutional and attention based capsule network to detect the driver's distraction," *IEEE Trans. Intell. Transport. Syst.*, vol. 24, no. 9, pp. 9561–9570, 2023.
- [19] M. Leekha, M. Goswami, R. R. Shah, Y. Yin, and R. Zimmermann, "Are You Paying Attention? Detecting Distracted Driving in Real-Time," in *International Conference on Multimedia Big Data*. IEEE, 2019, pp. 171–180.
- [20] Y. Xing, C. Lv, H. Wang, D. Cao, E. Velenis, and F.-Y. Wang, "Driver activity recognition for intelligent vehicles: A deep learning approach," *IEEE Trans. Veh. Technol.*, vol. 68, no. 6, pp. 5379–5390, Jun. 2019.
- [21] B. Qin, J. Qian, Y. Xin, B. Liu, and Y. Dong, "Distracted driver detection based on a cnn with decreasing filter size," *IEEE Trans. Intell. Transport. Syst.*, vol. 23, no. 7, pp. 6922–6933, 2022.
- [22] A. K. Dey, B. Goel, and S. Chellappan, "Context-driven detection of distracted driving using images from in-car cameras," *Internet Things*, vol. 14, 2021.
- [23] A. Behera, Z. Wharton, A. Keidel, and B. Debnath, "Deep cnn, body pose, and body-object interaction features for drivers' activity monitoring," *IEEE Trans. Intell. Transport. Syst.*, vol. 23, no. 3, pp. 2874–2881, 2022.
- [24] J. Wang, Z. Wu, F. Li, and J. Zhang, "A Data Augmentation Approach to Distracted Driving Detection," *Future Internet*, vol. 13, no. 1, 2021.
- [25] P. Li, M. Lu, Z. Zhang, D. Shan, and Y. Yang, "A Novel Spatial-Temporal Graph for Skeleton-based Driver Action Recognition," in *Intelligent Transportation Systems Conference*. IEEE, 2019, pp. 3243–3248.
- [26] A. Bera, Z. Wharton, Y. Liu, N. Bessis, and A. Behera, "Attend and Guide (AG-Net): A keypoints-driven attention-based deep network for image recognition," *IEEE TIP*, vol. 30, pp. 3691–3704, 2021.
- [27] C. Duan, Z. Liu, J. Xia, M. Zhang, J. Liao, and L. Cao, "Enhancing cross-dataset performance of distracted driving detection with score-softmax classifier," *arXiv preprint arXiv:2310.05202*, 2023.
- [28] S. Masood, A. Rai, A. Aggarwal, M. Doja, and M. Ahmad, "Detecting distraction of drivers using convolutional neural network," *Pattern Recognit. Lett.*, vol. 139, pp. 79–85, 2020.
- [29] W. Li, J. Wang, T. Ren, F. Li, J. Zhang, and Z. Wu, "Learning accurate, speedy, lightweight cnns via instance-specific multi-teacher knowledge distillation for distracted driver posture identification," *IEEE Trans. Intell. Transport. Syst.*, vol. 23, no. 10, pp. 17 922–17 935, 2022.
- [30] K. Peng, A. Roitberg, K. Yang, J. Zhang, and R. Stiefelhagen, "Trans-DARC: Transformer-based driver activity recognition with latent space feature calibration," in *IEEE Int. Conf. Intell. Rob. Syst. (IROS)*. IEEE, 2022, pp. 278–285.
- [31] B. Li, J. Chen, Z. Huang, H. Wang, J. Lv, J. Xi, J. Zhang, and Z. Wu, "A new unsupervised deep learning algorithm for fine-grained detection of driver distraction," *IEEE Trans. Intell. Transport. Syst.*, vol. 23, no. 10, pp. 19 272–19 284, 2022.
- [32] K. Han, Y. Wang, Q. Tian, J. Guo, C. Xu, and C. Xu, "Ghostnet: More features from cheap operations," in *CVPR*. IEEE/CVF, 2020, pp. 1580–1589.
- [33] N. Siddiqui, P. Tirupattur, and M. Shah, "Dvanet: Disentangling view and action features for multi-view action recognition," in *Conference on Artificial Intelligence*, vol. 38, no. 5. AAAI, 2024, pp. 4873–4881.
- [34] F. Schroff, D. Kalenichenko, and J. Philbin, "Facenet: A unified embedding for face recognition and clustering," in *Conference on Computer Vision and Pattern Recognition*. IEEE, 2015, pp. 815–823.
- [35] A. Howard, M. Sandler, G. Chu, L.-C. Chen, B. Chen, M. Tan, W. Wang, Y. Zhu, R. Pang, V. Vasudevan *et al.*, "Searching for mobilenetv3," in *ICCV*. IEEE/CVF, 2019, pp. 1314–1324.
- [36] F. N. Iandola, S. Han, M. W. Moskewicz, K. Ashraf, W. J. Dally, and K. Keutzer, "Squeezenet: Alexnet-level accuracy with 50x fewer parameters and 0.5 mb model size," *preprint arXiv:1602.07360*, 2016.
- [37] Z. Zhong, L. Zheng, G. Kang, S. Li, and Y. Yang, "Random erasing data augmentation," in *AAAI Conference on Artificial Intelligence*, vol. 34, 2020, pp. 13 001–13 008.



Simone Bianco is currently an Associate Professor of computer science with the University of Milano-Bicocca, Milan, Italy. He is on Stanford University's World Ranking Scientists List for his achievements in Artificial Intelligence (AI) and Image Processing. His teaching and research interests include computer vision, AI, Machine Learning (ML), optimization algorithms applied in multimodal, and multimedia applications. He is also a R&D Manager of the University of Milano-Bicocca spin-off Imaging and Vision Solutions, and Member of European Laboratory for Learning and Intelligent Systems (ELLIS Society).



Luigi Celona is an Assistant Professor of computer science at the University of Milano-Bicocca, Italy. In 2018 and 2014, he obtained respectively the PhD and the MSc degree in Computer Science at DISCo. In 2011, he obtained the BSc degree in Computer Science from the University of Messina. His current research interests focus on image analysis and classification, ML and face analysis. He is a member of the European Laboratory for Learning and Intelligent Systems (ELLIS Society). He is the Conferences Liaison of the IEEE CTSoc Machine Learning, Deep Learning and AI in CE (MDA) Technical Committee (TC).



Paolo Napolitano (Member, IEEE) is an Associate Professor of computer science at the University of Milano-Bicocca, since 2021. His main research interests include AI, ML and DL, CV, PR, intelligent sensors, biological signal processing, and human-machine systems. He is a member of the European Laboratory for Learning and Intelligent Systems (ELLIS Society). He is an Associate Editor of IEEE JOURNAL OF BIOMEDICAL AND HEALTH INFORMATICS, *Neurocomputing* (Elsevier), *IET Signal Processing*, *Sensors* (MDPI), and *Smart Cities* (MDPI). He is the Chair of the IEEE CTSoc Machine Learning, Deep Learning and AI in CE (MDA) Technical Committee (TC).